Journal of the Brazilian Society of Mechanical Sciences and Engineering (2018)40:87
https://doi.org/10.1007/s40430-018-1008-9

TECHNICAL PAPER

Dependence of plastic strain and microstructure on elastic modulus reduction in advanced high-strength steels

Sérgio Fernando Lajarin[1] · Chetan P. Nikhare[2] · Paulo Victor P. Marcondes[1]

Received: 19 June 2017 / Accepted: 28 October 2017

Abstract
Increase in the use of the advanced high-strength steels (AHSS) is an interesting alternative to automotive industry to reduce vehicle weight and fuel consumption. However, it has been limited due to challenges in formability, tool life, and springback. The springback is pointed in the literature as one of the challenges that involves the mass production of structural components and the aspects that shows influence are still not fully understood. There is still a gap in the literature to analyze the elastic modulus variation during unloading (also called chord modulus). Therefore, this study experimentally examines the variation of elastic modulus in conjunction with plastic strain and initial microstructure of various automotive steels. For all AHSS, it was found that the elastic modulus decreases during loading and unloading with respect to plastic strain. It was observed that the microstructure of AHSS greatly affects the reduction in elastic modulus upon deformation. It was also found that the degradation of elastic modulus also affected by the anisotropy of the material.

Keywords Advanced high-strength steel · Springback · Elastic modulus · Microstructure · Anisotropy

1 Introduction

In recent decades, the automotive industry is undergoing through a great international pressure to adapt environmental requirements and reduce emissions of green house gases in the atmosphere. One of the alternatives explored is the reduction of fuel consumption by reducing the weight of the vehicles using thinner sheet metal or lighter materials. However, to reduce the sheet thickness without compromising the safety aspects, such as the impact absorption capability [1], the automotive industry has maintained effort to test other types of steels.

The conventional steels of low- and high-strength hare widely used to manufacture automotive bodies. These steels do have large deformation capacity, but are limited in applications due to lower strength. The high-strength low alloy steel (HSLA) provides greater mechanical strength than low carbon steels allied with medium formability. Aiming to maintain the dominance use of steels in vehicles, the development of advanced high-strength steels (AHSS) was proposed. The two most popular steels in this group are DP (dual phase) and TRIP (TRansformation-Induced Plasticity) steels [2, 3]. These steels ensure higher strength than conventional steels combined with high ductility [4]. However, its wide application in the automotive industry is still limited due to the challenges in formability, sheet metal coupling, tool life, and springback behavior. The springback is the main problem which compromises the mass production of automotive structural components with AHSS [5–11]. The same phenomenon also called as elastic recovery is identified as a change occurred in the shape of the component after the forming tool removal, caused by redistribution of the residual elastic stress [12–14].

The phenomenon of variation inelastic behavior during the unloading has been first experimented in [15]. The decrease in the elastic modulus for various types of steel after pre-strained was investigated and found that the elasticity can decrease 17.5% of its initial value after 5% of

Technical Editor: Márcio Bacci da Silva.

✉ Paulo Victor P. Marcondes
marcondes@ufpr.br

[1] DEMEC, Universidade Federal do Paraná, Av. Cel. Francisco H. dos Santos, 210, Caixa Postal 19011, Curitiba, Paraná CEP 81531-990, Brazil

[2] Department of Mechanical Engineering, The Behrend College, The Pennsylvania State University, Erie, PA 16563, USA

Published online: 29 January 2018

plastic strain for high-strength steels [16]. The non-linearity of elastic recovery in unloading of high-strength steel was noted [17]. It was mentioned that the movement and pile-up of dislocations caused by plastic strain are the cause of the variation of elastic modulus during unloading [16–19] (also called chord modulus). During deformation, free dislocations move along the slip planes and are easily piled when barred by solutes, grain boundaries, or other obstacles. These pile-ups of dislocations can return when the shear stress is removed during unloading, leading to a small portion of elastic strain. Such effects arise from mobile dislocations which can move in response to the internal repulsive forces between them when the external forces on the material were removed. Further breakup of dislocation tangles and cell walls will also release more mobile dislocations during unloading and reverse loading. Since the density of dislocations in a solid increase with increase in forming strain, this non-linear springback contribution also increases with increasing forming strain. Upon characterization of elastic response for two commercial low-alloyed TRIP steels, it was concluded that the variation of elastic modulus in unloading observed is attributed mainly to micro-plastic strain caused by displacement of mobile dislocations [17, 20, 21]. The increase in micro-plastic strain was observed in DP590 steel as compared to mild steel 270 with respect to the pre-strained value [22]. This difference in the micro-plastic strain noted to be attributed with respect to their microstructure as mobile dislocation said to be easier in ferrite than in martensite, which shows the difference in micro-plastic strain during unloading. Conventional steel been mostly ferrite and AHSS has a combination of ferrite, austenite, bainite, and martensite; however, very limited reporting is available on how variation in elastic modulus depends on microstructure.

Due to the complex nature of AHSS microstructure, anisotropy could be easily involved and would show change in material behavior in various directions. For DP steel, it was found that the degradation of elastic modulus is different in 0°, 45°, and 90° to rolling direction [23]. Limited data on these parameters would make it difficult to describe the correct material behavior for finite-element analysis during loading and unloading deformation and failed to reach accuracy [5, 14, 24–34]. The influence of computational parameters in the springback simulation was studied and mentioned the need of adequately characterize material nonlinearity [35]. The phenomenon of variation inelastic modulus during unloading has been cited as a major cause of nonlinearity behavior of these steels [36].

As noticed, there is still a gap in the literature to analyze the elastic modulus variation during unloading. Therefore, the objective of this study is to characterize experimentally the reduction in elastic modulus during loading and unloading and its relation with the plastic strain and microstructure. The anisotropy was observed in the material and was characterized and discussed. The variation of the elastic modulus during unloading and loading was observed for all the studied steels and consideration regarding the correlation with the microstructure was made.

2 Materials and methods

2.1 Materials

The sheet materials studied were various grades of steel commonly used in the automotive industry (Table 1). The mild steel DC05 and HSLA have been used for many years in the production of automotive body structures. DC05 is low-strength steel, while HSLA is higher strength steel which is primarily obtained by micro-additions of micro-alloying elements used to control the grain size. The AHSS utilized consisted of three dual-phase steels (DP) with a range of ultimate tensile strengths of 600, and 980 MPa and a TRansformation-Induced Plasticity steel (TRIP) with ultimate tensile strength of 780. The steels were obtained from two suppliers (A and B) with thicknesses between 1.5 and 2 mm. The material surface condition was galvanized.

2.2 Uniaxial tensile test

The uniaxial tensile tests were prepared and performed according to NBR standard 6673 [37] (Fig. 1). Tensile tests were carried out at orientations of 0°; 45°, and 90° to the rolling direction and pulled at a nominal strain rate of $\sim 10^{-4}$/s. Three specimens in each rolling direction were tested until failure to plot the stress–strain curve. The following mechanical properties were analyzed: initial elastic modulus (E_0), yield strength (YS), and ultimate tensile strength (UTS). In addition, three more specimens in each rolling direction were tested until 12% strain for all materials except 18% for DC05 and 6% for DP980 to calculate the Lankford anisotropy parameters such as

Table 1 Material grades, commercial thicknesses and chemical composition

Material	Thickness (mm)	Supplier	Chemical composition		
			C	Si	Mn
DC05	1.50	A	0.06	0.10	0.35
HSLA490	1.57	A	0.08	0.03	0.60
DP600-A	1.50	A	0.14	0.40	2.10
DP600-B	1.50	B	0.086	0.053	1.739
DP980	1.52	B	0.154	0.047	2.224
TRIP780	2.00	A	0.25	–	2.0

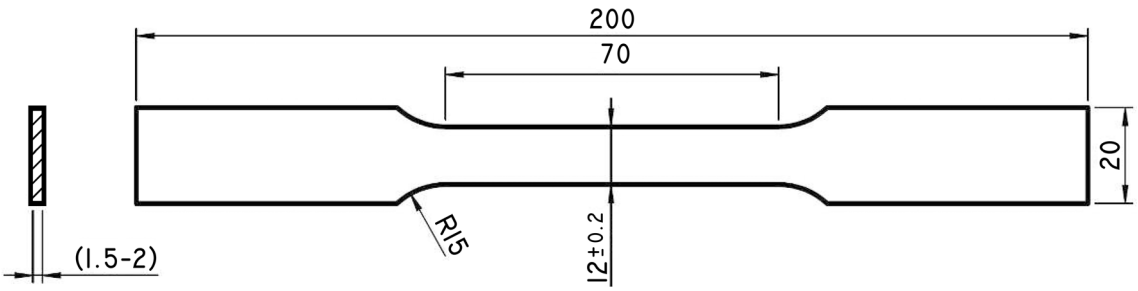

Fig. 1 Geometry of specimen for tensile test (all dimensions are in mm)

normal r value, planar Δr value, and normal r medium-value (r_m) coefficients. All tensile tests were conducted using a universal testing machine EMIC® at room temperature ($\sim$ 20 °C) and the strain was measured using an extensometer.

2.3 Microstructural analysis

The microstructural analysis procedure can be simplified in the following steps: (1) mounting a sample of the material; (2) grinding by means of four different sand paper granulations; (3) polishing with alumina; (4) etching with Nital 2% ($C_2H_5OH + HNO_3$); and (5) optical micrograph investigation.

2.4 Determination of the variation of the elastic modulus during unloading

To characterize the elastic behavior, monotonic uniaxial tensile tests were followed by unloading with a nominal strain rate of $\sim 10^{-4}$/s. Nine trials for each material were made, three being in each rolling direction. The specimen was initially elongated to a plastic strain of about 0.5% and then unloaded. Furthermore, the reloading and unloading processes were repeated using the following strain increment of: 1% until 7.5%; then 2% until 13.5%; and then 3% until failure. After each unloading, the specimen rested for 1 day at room temperature to relieve the imposed residual stresses [20]. A low strain increment (i.e., 1%) at the start was applied as most variation in elastic modulus happens between 0 and 5% strain [16], and later, it tends to stabilize. At each loading and unloading, the elastic modulus was measured and plotted.

3 Results and discussion

3.1 Mechanical properties

Figure 2 shows the difference in the behavior of the stress–strain curve for analyzed materials, and Tables 3, 4, and 5 summarize the mechanical properties. Both grades of DP steel showed higher initial work hardening. e., up to 7%, and later stabilized. DP600 have shown uniform and total elongation in a superior level to that showed by HSLA steel. Also seen that the YS is similar to the HSLA but with much higher UTS. Curiously, the DP600 steel from suppliers A and B, although of similar grade, showed different behavior between them. The steel from supplier B showed higher elongation and a slight level of elastic–plastic transition similar to HSLA. Moreover, the steel from supplier A showed a high initial work hardening for dual-phase steel and a quick stabilization resulting in an elongation of 0.9% lower. DP980 steel showed uniform elongation of 7%, which can be considered high for steel with such ultra-high strength.

From a practical standpoint, the TRIP780 steel showed a positive characteristic, i.e., low YS/UTS ratio- around 0.63. As can be seen, the large margin between the YS and UTS may be beneficial for stamping operations, Fig. 2. The initial hardening coefficient of TRIP was lower than that of DP steel, but lasts longer and achieved a uniform elongation of 22.6% close to the DC05 steel.

Table 2 shows the anisotropic mechanical properties of the materials. The steel with greater ability to resist thinning when subjected to tension and/or compression stresses in the plane is the DC05 steel with r_m of 1.572 and the lowest is the DP600-A with r_m of 0.820.

All materials presented here show normal and planar anisotropy. The HSLA490 steel showed the lowest Δr and the DC05 steel presented the largest. This parameter indicates the difference of mechanical behavior in the plane of the sheet. The materials with $\Delta r(+)$ indicate a trend to earing in longitudinal and transverse directions of rolling, while the materials with $\Delta r(-)$ indicate earing in the 45^0 direction.

3.2 Elastic modulus obtained during unloading

The variation inelastic modulus with respect to plastic strain was reported by Lems [15]. In this work, in an attempt to assess the magnitude of this effect, cyclic

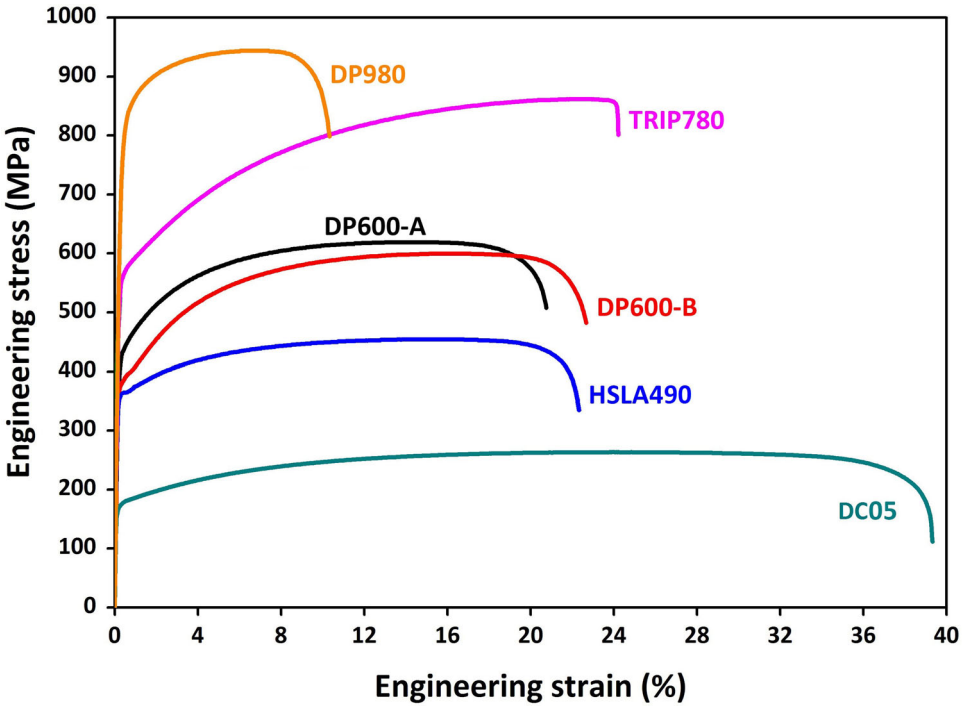

Fig. 2 Stress–strain curves for different engineering degrees of high-strength steels and a conventional steel of low strength

Table 2 Anisotropic properties for tested materials

Steels	r_0	r_{45}	r_{90}	Δr	r_m
DC05[a]	1.958	1.354	1.624	0.436	1.572
HSLA 490	0.777	0.876	0.903	− 0.036	0.858
DP600-A	0.835	0.676	1.088	0.285	0.820
DP600-B	0.638	1.097	0.802	−0.377	0.909
DP980[b]	0.875	1.038	0.932	−0.134	0.971
TRIP780	0.847	0.902	1.092	0.068	0.936

All other materials were obtained from $\varepsilon = 0.12$

[a]Obtained from $\varepsilon = 0.18$

[b]Obtained from $\varepsilon = 0.06$

loading–unloading tensile tests for five different materials were performed at as train rate of $\sim 10^{-4}$/s.

Figure 3a shows the curves for different percents of plastic deformation for the conventional steel HSLA490. The elastic modulus during unloading was obtained by dividing the stress before unloading by the total recovered strain at zero stress, Fig. 3b. The unloading elastic modulus in 0°, 45°, and 90° to rolling direction as well as for the average of three directions with respect to different plastic strain percent is shown in Fig. 3c. All curves were fitted with the exponential formula (Eq. 1) presented in [38, 39]

$$E_{av} = E_0 - (E_0 - E_{sat})\left[1 - \exp\left(\xi\varepsilon_0^p\right)\right] \quad (1)$$

where E_0 initial elastic modulus; E_{sat} saturated elastic modulus after prestrain; ε_0^p prestrain value; ξ a material parameters indicating the modulus decay rate.

The instantaneous elastic modulus obtained during unloading decreased from 207 to 173 GPa, representing 16.4% of decrease.

Figures 4, 5, 6, and 7 show the variation of the elastic modulus obtained during unloading of the, DP600-A, DP600-B, DP980, and TRIP780 steels.

Tables 3, 4, and 5 provide the initial elastic modulus, saturated modulus, the calculated material parameter, and percentage reduction in modulus (%RE) from initial to saturation in 0°, 45°, and 90° to rolling direction. It indicates that the TRIP steel provides the highest drop in elastic modulus, followed by DP600-B, DP600-A, DP980, and HSLA.

Further observations related to elastic anisotropy were noted in all materials. For HSLA490, the less reduction in elastic modulus was observed in transverse direction than 45° and then 0° for same strain. At 0.09 and above strain, the elastic modulus seems saturated and very close to each other (Fig. 3c). This can also be noted from Δr value. Δr value is close to zero for this material; Table 2 indicates little to no anisotropy. However, the decrease in elastic modulus differences is higher prior to 12% strain (Fig. 3c), but shows less anisotropic effect at 12% for which strain Δr value was captured. Prior to 12% strain, the material is believed to be highly anisotropic with higher negative Δr value which indicates than material was softer in 45° than other two directions and found higher decrease in elastic modulus. With DP600-A, the trend is an outlier in all. It shows less reduction in elastic modulus for 45° than 90° than 0° until strain of 0.07 and then saturated until

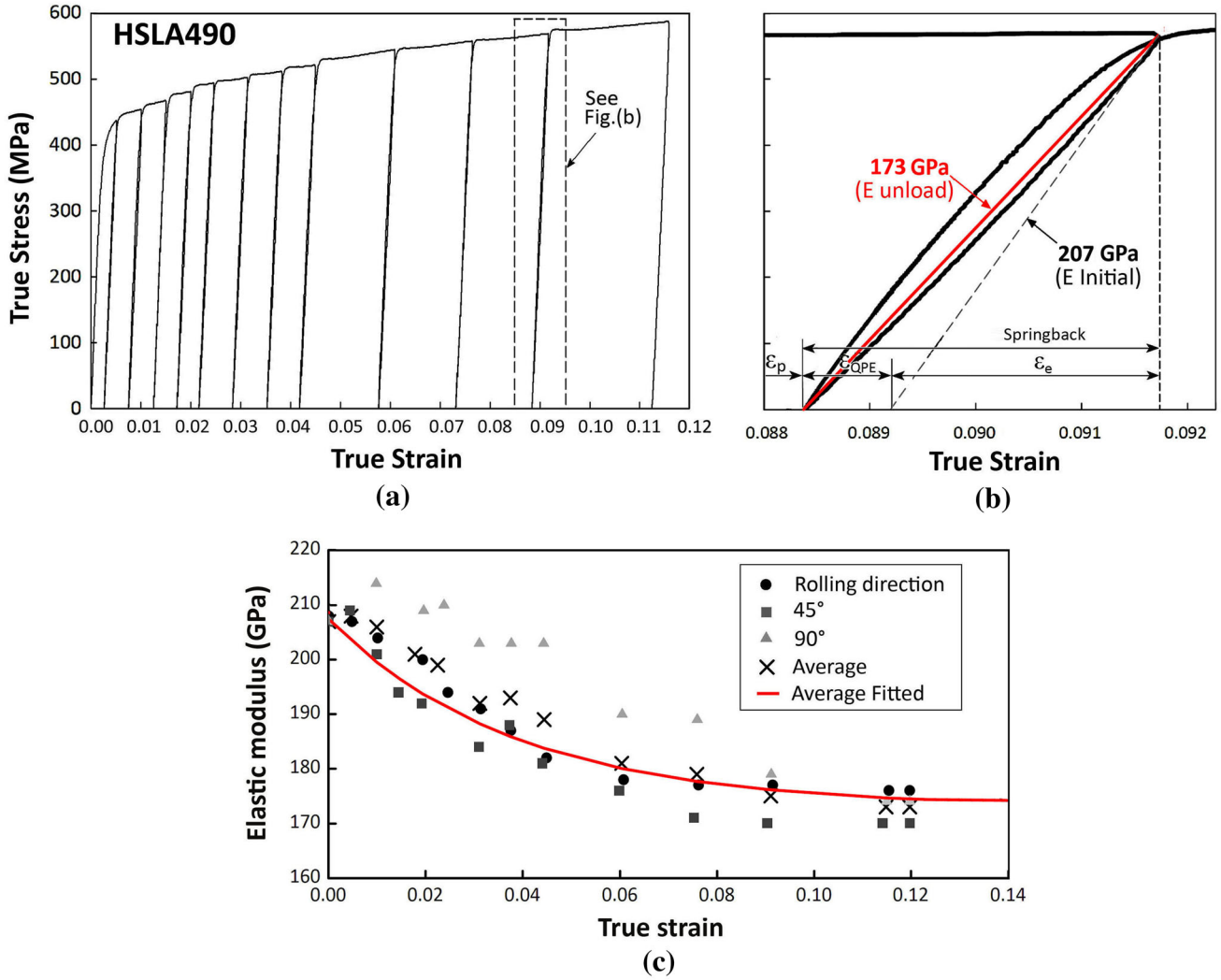

Fig. 3 Unloading–loading cycles obtained from the uniaxial tensile tests: **a** HSLA490, **b** detail showing the behavior of the unloading elastic modulus and **c** measured elastic modulus at various strains

0.09. After 0.09, the trend is flipped and less reduction occurred with 0° than 90° than 45° (Fig. 4c) with no saturation until failure. This observation was also supported with given positive Δr value (Table 2), which suggests that 0° than 90° direction material was softer and thus higher decrease in modulus was found. Similar observations were found for DP600-B, DP980, and TRIP780. When observing DP600-B, the 90° sample gets less reduction in elastic modulus than 0° than 45°. In this grade, no saturation occurred until failure (Fig. 5c). For DP980, the trend is similar as DP600-B, and in this case too, no saturation occurred until failure (Fig. 6c). With TRIP780, the 45° sample shows less reduction in elastic value than 90° than 0° with no saturation until failure (Fig. 7c). Table 6 provides the detail outlook related to elastic anisotropy and the approximate elastic difference at any strain. The elastic difference is the difference of minimum and maximum directional (0°, 45°, and 90° to rolling direction) unloading elastic modulus. The saturation is the region where directional anisotropy in unloading elastic modulus disappeared.

3.3 Microstructure characteristics

Figure 8 illustrates the as received micrographs of the tested steels. The first two (Fig. 8a, b) are conventional ferritic steels with polygonal grains. Steel DC05 (Fig. 8a) is the one that showed larger and more uniform grains, around 20 μm, against 8.34 μm of HSLA490 steel.

The other materials are AHSS steels that unlike the conventional steels and show one or more phases associated with the ferritic matrix. In DP600 steels (Fig. 8c, d), martensite islands are concentrated in the grain boundaries. As can be seen, in Table 7, the DP600-A and B steels presented, respectively, 83.4 and 85.8% of ferrite, 15.6 and

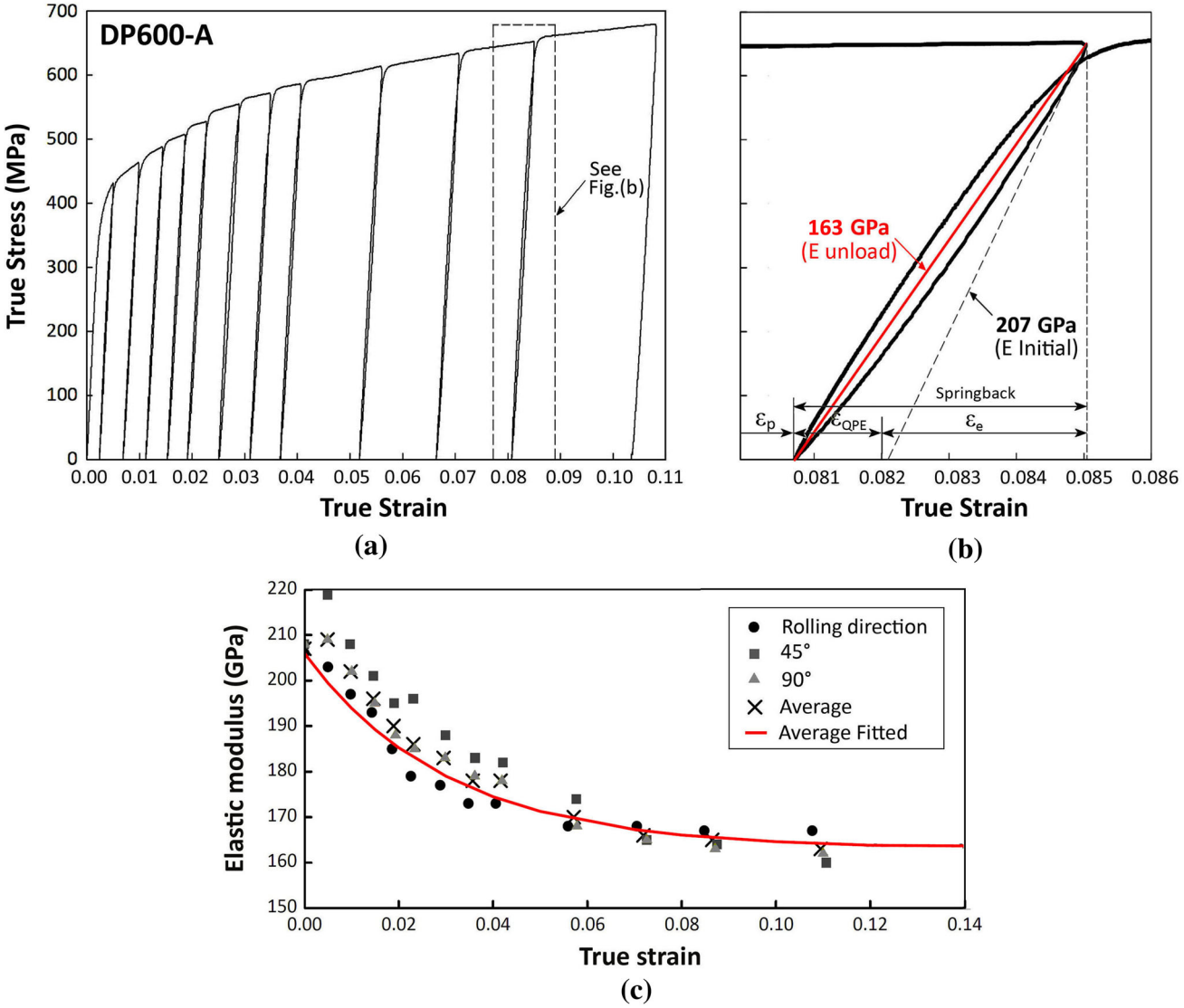

Fig. 4 Unloading–loading cycles obtained from the uniaxial tensile tests: **a** DP600-A, **b** detail showing the behavior of the unloading elastic modulus and **c** measured elastic modulus at various strains

13.1% of martensite, and 0.9 and 1.1% of bainite. Oliver et al. [40] measured around 13.4% of martensite and 1.1% of bainite in the same grade of steel and ferrite grains with an average size of 5.68 µm. In DP600-A (Fig. 8c), the average size of ferrite grains was 5.92 µm, while for the DP600-B, Fig. 5d was 5.04 µm.

The combination of soft ferrite matrix and the martensitic hard ''islands'' guarantee to the DP steels high formability and high strength. Even though the grain size for DP600-A is bigger than DP600-B, the higher stress and lower elongation were achieved, which should be opposite. This behavior is due to the higher martensite percentage in this material. DP980 steel (Fig. 8e) shows inter-granular ferrite in a martensitic matrix which is different than DP600 steel, ensuring high value of UTS for the material. Table 7 details the volume fraction of ferrite, martensite, bainite, and retained austenite along with grain size and feret ratio—which is the ratio between the length and width of the grains.

Figure 8f shows the TRIP780 steel micrograph. However, due to difficulty in achieving the perfect etch for this material, the metallographic phases could not be quantified. Oliver et al. [40] managed to reveal quite successfully the TRIP steel phases of the same grade and the authors measured 72.4% ferrite, 13.9% of retained austenite, 10.4% of bainite and 3.3% of martensite, and average grain size of ferrite of 4.34 µm. The retained austenite transforms to martensite when the material is plastically deformed and these characteristics ensure to the steel excellent formability properties.

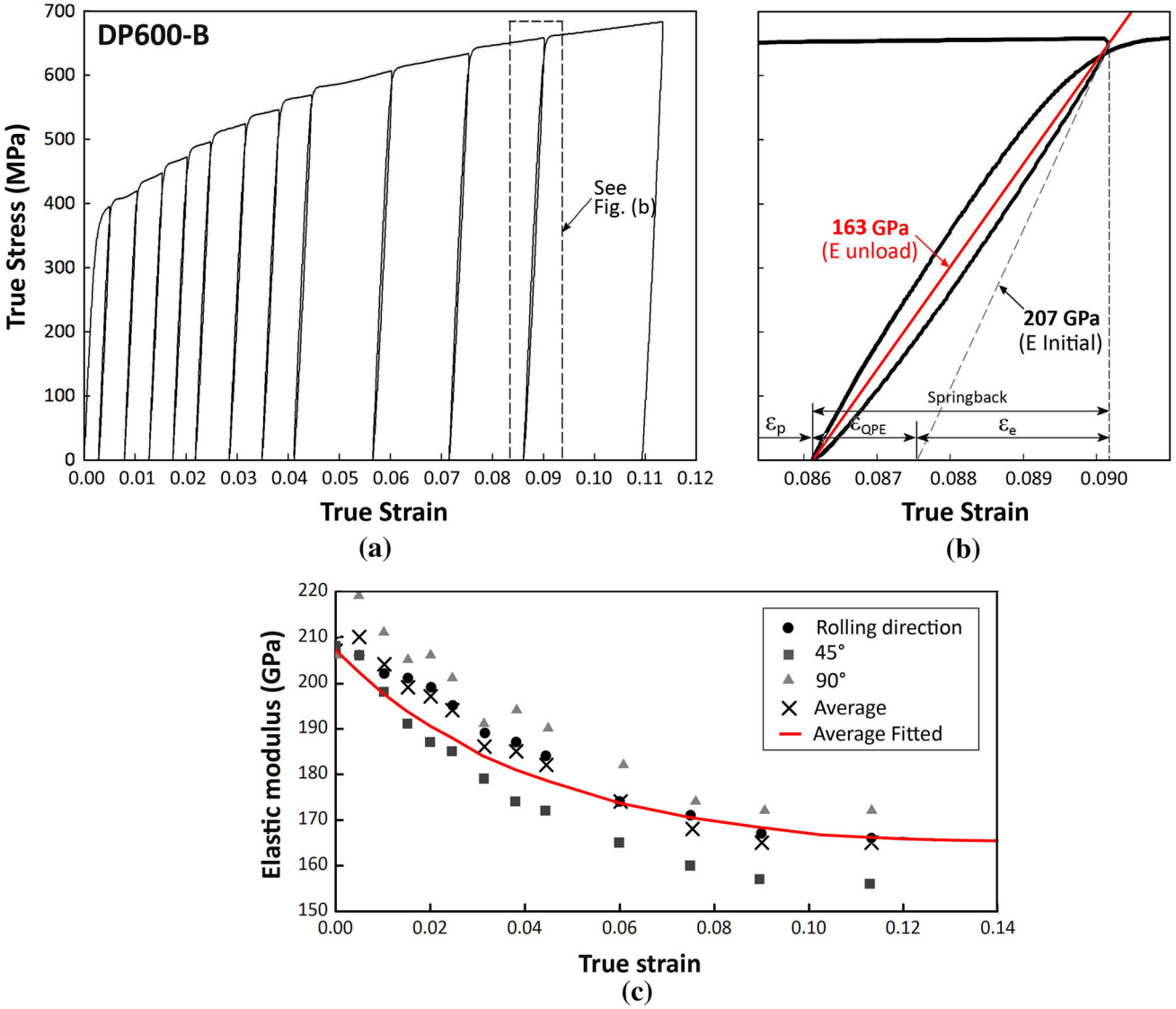

Fig. 5 Unloading–loading cycles obtained from the uniaxial tensile tests: **a** DP600-B, **b** detail showing the behavior of the unloading elastic modulus and **c** measured elastic modulus at various strains

All materials reflected with initial modulus of elasticity between 205 and 212 GPa, typical range value of carbon steel. In Fig. 9, the curves of the elastic modulus behavior during unloading versus the plastic strain of all tested materials in rolling direction are shown. The curves represent actual experimental data point in rolling directions.

Except DP980 steel all other tested advanced high-strength steels showed higher reduction in modulus of elasticity with respect to their strength. The TRIP780 steel which had the highest tensile strength after DP980 among all tested materials showed the higher reduction in modulus of elasticity during unloading, followed by DP600-A, DP600-B steels and finally the conventional HSLA steels. Eggertsen and Mattisson [42] found similar results where they analyzed two DP600 steels and two low carbon steels: DX56 and 220IF, and found greater reduction in modulus of elasticity for the higher strength steels. Similar trend has seen in [22] when compared DP with mild steel. This relationship is comprehensive considering that the greater the strength at the point immediately prior to unloading, the greater the non-linear elastic recovery (discussed in the above figures), and consequently, small will be the slope of the secant line that indicates the modulus of elasticity in unloading and after loading. If closely observed a single unload and load curve, it can be noted that start of unload curve has higher modulus than end of unload curve. This phenomenon is the same for load curve, i.e., higher modulus at start than at end. This phenomenon describes that the similar mechanics is happening in both unloading and loading. However, in loading, the relaxation of micro-

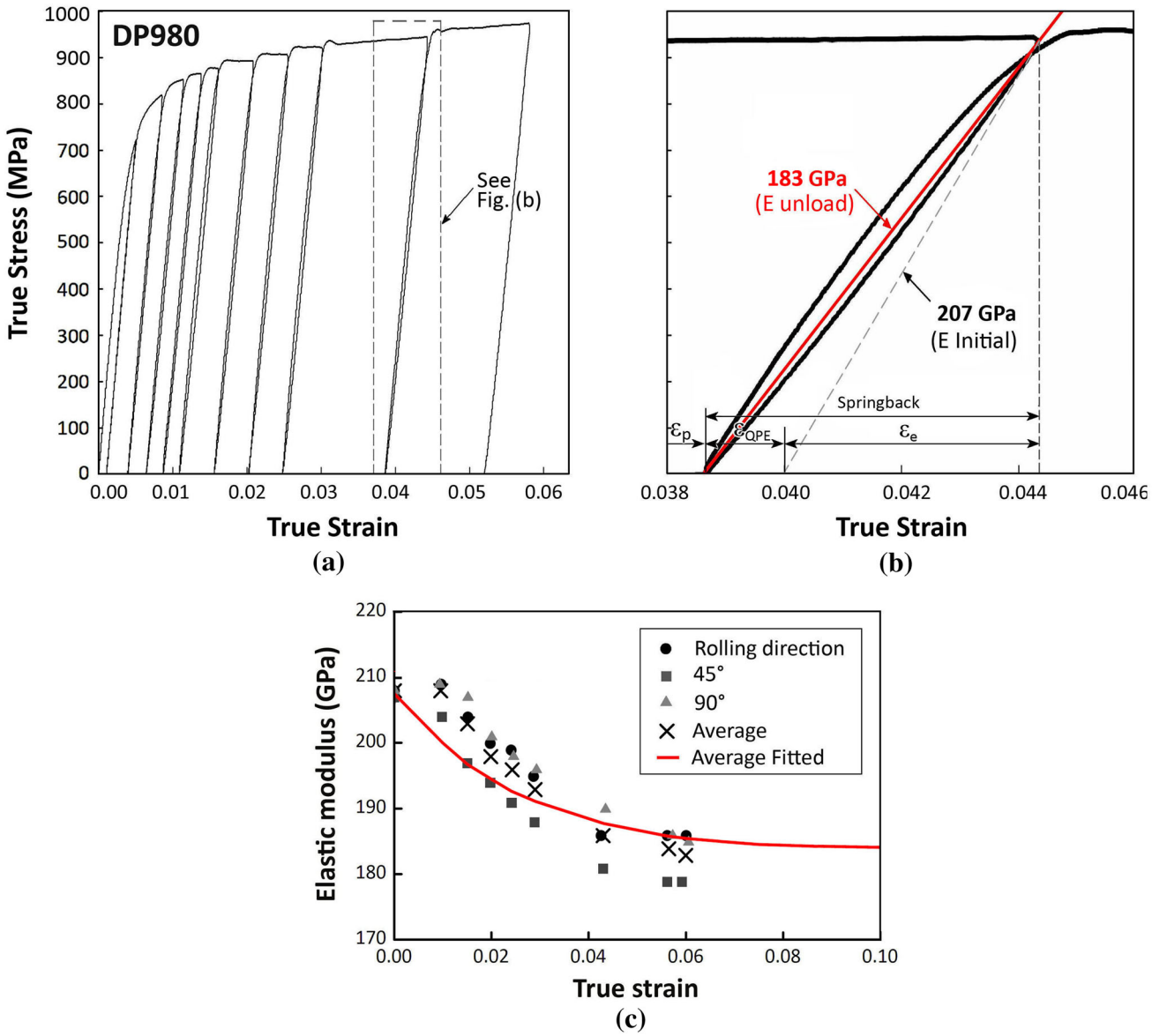

Fig. 6 Unloading–loading cycles obtained from the uniaxial tensile tests: **a** DP980, **b** detail showing the behavior of the unloading elastic modulus and **c** measured elastic modulus at various strains

plastic strain happens first and then dislocation been pushed and stored in pile-ups. However, this result is contrary to that obtained by Cobo et al. [36] that analyzed different grades of DP steels and reported that less degradation occurred for higher strength. In their case, the main microstructural difference between the steels studied was the amount of ferrite. The pearlite was neglected due to significantly lesser in amount [36, 40]. For lower strength DP, the ferrite volume fraction was 75%, but for high-strength DP, it was only 10% in martensite matrix and the conclusion made was that the reduction in modulus of elasticity decreases as the ferrite volume fraction decreases. The justification made was the fact that the dislocation movement is easier in body-centered cubic ferritic structure than in martensite. Thus, the local micro-plastic strain is in smaller quantities when the material has higher ferrite volume fraction. In contrast, the higher martensite volume fraction in the microstructure will generate higher plastic micro-strain. This is due to the different elastic back stresses of different phases. Martensite is believed to have higher back stress (due to higher strength) compared to ferrite and generates higher residual stresses in ferrite/martensite interface. This increase in residual stress increases in the degradation of elastic modulus. With this fact, DP600-A should have higher reduction in elasticity than DP600-B, but the results are opposite. The grain size in DP600-A is 5.92 μm compared to 5.04 μm in DP600-B. This factor increases the grain boundaries and thus

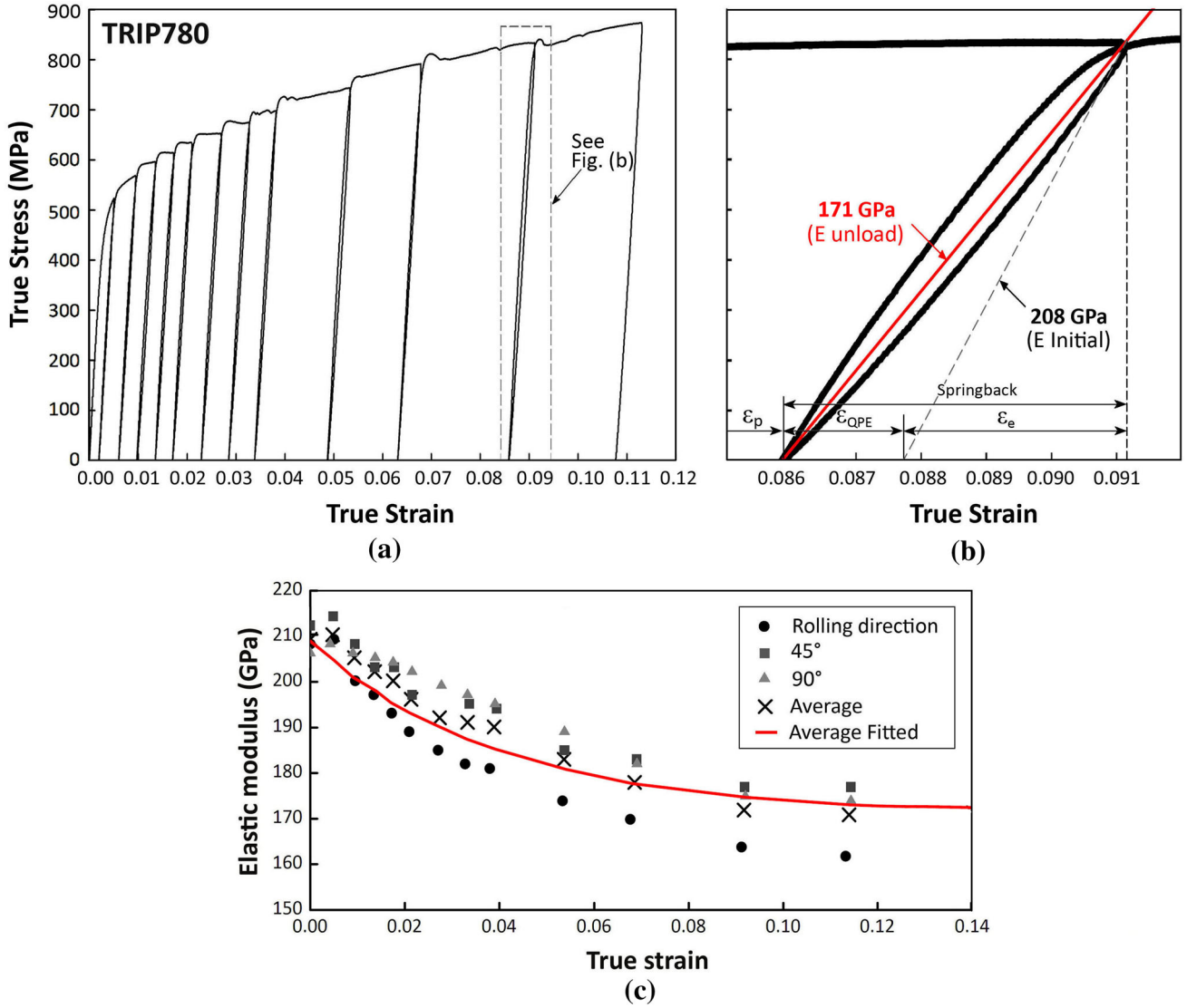

Fig. 7 Unloading–loading cycles obtained from the uniaxial tensile tests: **a** TRIP780, **b** detail showing the behavior of the unloading elastic modulus and **c** measured elastic modulus at various strains

Table 3 Elastic reduction and comparison with mechanical properties in 0° to rolling direction

Steels	E_0 (GPa)	E_{sat} (GPa)	ξ	%RE	YS (MPa)	UTS (MPa)	n	K	Total El (%)
HSLA 490	207.1	176.4	31.5	14.8	407	540	0.126	796	20.8
DP600-A	206.4	166.6	51.5	19.3	399	618	0.154	957	20.8
DP600-B	207.1	165.3	24.0	20.1	382	595	0.185	999	22.7
DP980	207.9	185.0	32.0	11.0	857	934	0.075	1224	11.4
TRIP780	208.0	161.8	27.5	22.2	523	854	0.255	1568	28.5

YS yield strength; *UTS* ultimate tensile strength; *Total EI* total elongation; n strain hardening coefficient; K strength coefficient, both n and K obtained from $0.04 < \varepsilon < 0.12$

[a]Obtained from $0{:}04 < \varepsilon < 0.20$

[b]Obtained from $0.03 < \varepsilon < 0.06$

Table 4 Elastic reduction and comparison with mechanical properties in 45° to rolling direction

Steels	E_0 (GPa)	E_{sat} (GPa)	ξ	%RE	YS (MPa)	UTS (MPa)	n	K	Total El (%)
HSLA 490	207.4	168.5	29.5	18.7	411	523	0.115	752	21.7
DP600-A	208.0	160.0	24.5	23.1	403	624	0.148	965	19.5
DP600-B	208.2	155.7	29.5	25.2	386	602	0.190	1000	24.9
DP980	206.7	179.1	44.5	13.3	810	923	0.078	1220	9.3
TRIP780	212.1	176.6	26.5	16.7	558	862	0.252	1585	24.2

YS yield strength; *UTS* ultimate tensile strength; *Total EI* total elongation; n strain hardening coefficient; K strength coefficient, both n and K obtained from $0.04 < \varepsilon < 0.12$

[a]Obtained from $0{:}04 < \varepsilon < 0.20$

[b]Obtained from $0.03 < \varepsilon < 0.06$

Table 5 Elastic reduction and comparison with mechanical properties in 90° to rolling direction

Steels	E_0 (GPa)	E_{sat} (GPa)	ξ	%RE	YS (MPa)	UTS (MPa)	n	K	Total El (%)
HSLA 490	206.2	173.9	16.5	14.2	427	563	0.110	795	18.1
DP600-A	208.1	162.0	28.5	22.1	385	616	0.153	978	19.9
DP600-B	205.9	167.2	18.0	18.8	396	622	0.186	1030	20.8
DP980	207.9	185.4	34.0	10.8	815	944	0.080	1252	10.4
TRIP780	205.6	174.5	21.0	15.1	563	864	0.25	1595	20.4

YS yield strength; *UTS* ultimate tensile strength; *Total EI* total elongation; n strain hardening coefficient; K strength coefficient, both n and K obtained from $0.04 < \varepsilon < 0.12$

[a]Obtained from $0{:}04 < \varepsilon < 0.20$

[b]Obtained from $0.03 < \varepsilon < 0.06$

Table 6 Elastic anisotropy

Steels	Trend	Elastic difference (%)	Saturation	Flipped	Elastic difference	Saturation
HSLA490	90-0-45	~ 15	Yes at 0.09 until failure	–	–	–
DP600-A	45-90-0	~ 10	Yes between 0.07 to 0.09	Yes; trend: 0-90-45	~ 7	No until failure
DP600-B	90-0-45	~ 20	No until failure	–	–	–
DP980	90-0-45	~ 7	No until failure	–	–	–
TRIP780	45-90-0	~ 15	No until failure	–	–	–

Trend 90-0-45 means elastic reduction less for 90° than 0° than 45° at same strain value and respectively

dislocation density in DP600-B even if the martensite volume fraction is lower. Due to increase in dislocation density, the micro-plastic strain believed to be higher than in DP600-A and thus increases the reduction in elasticity.

The justification given by Cobo et al. [36] serves to explain the DP980 steel behavior, as shown in Fig. 9. As can be seen in the micrograph of this steel illustrated in Fig. 8e, it shows a large percentage of inter-granular ferrite in martensitic matrix. Due to which the back stress of martensite and ferrite would not have generated the overall amount of residual stresses at ferrite/martensite and martensite/martensite interface. Thus, lower micro-plastic strain evolved and resulted in lesser degradation of elastic modulus. This in fact was responsible for less reduction (13.5%) in elastic modulus during unloading.

It is reported that with increase in plastic strain, the micro-cracks increases, thus reduces the density of material, and thus decrease the elasticity [22] in general. This fact believed to be directly applicable to TRIP steel, where the volume of material increases [43] due to transformation of austenite to martensite during plastic deformation. In TRIP780 steel, the austenite volume fraction noted was 13.9%. The transformation of austenite starts quickly with deformation at low carbon levels, but more stable in high

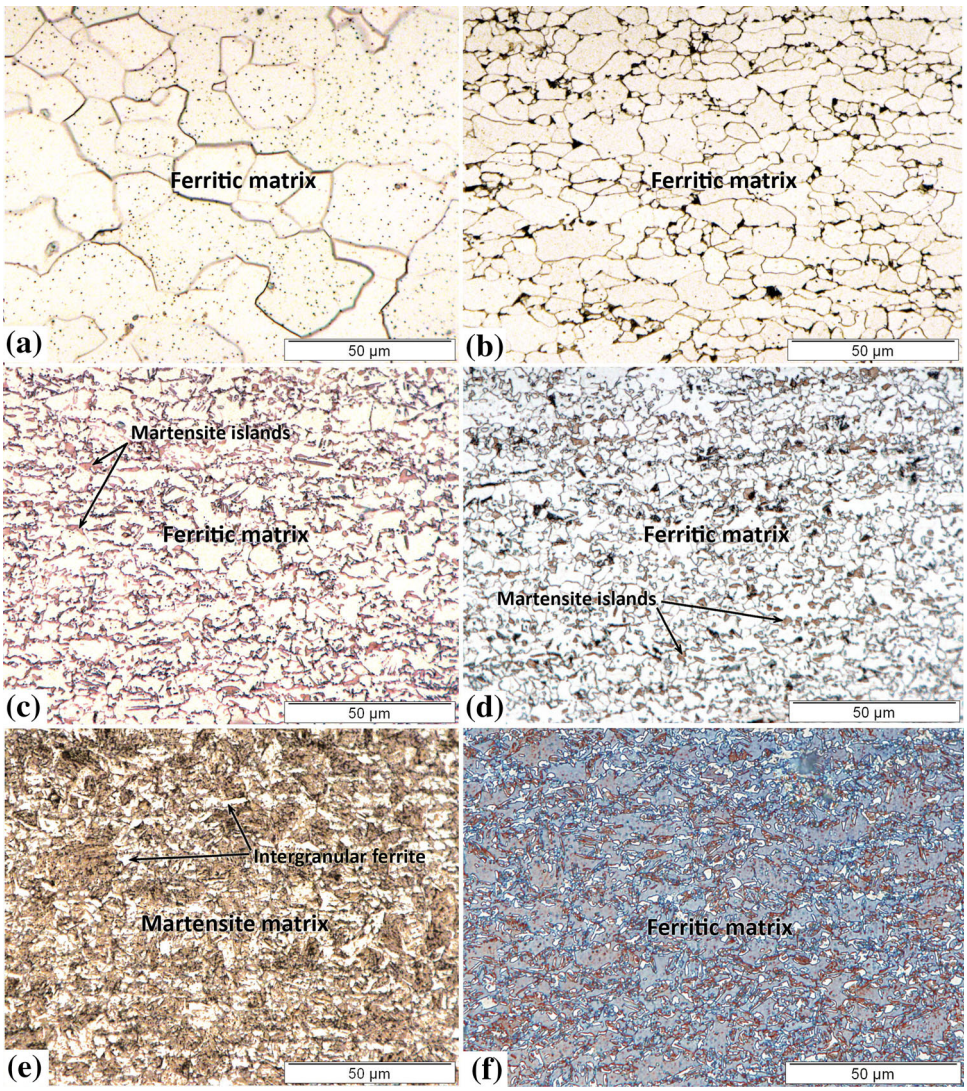

Fig. 8 Optical micrographs of steels: **a** DC05; **b** HSLA490; **c** DP600-A; **d** DP600-B; **e** DP980 and **f** TRIP780

Table 7 Quantitative metallography results

Grade	Volume fraction (%)				Grain size (µm)	Feret ratio
	Ferrite	Martensite	Bainite	Retain. Aust.		
DC05	–	–	–	–	20.06	1.32
HSLA 490	–	–	–	–	8.34	1.95
DP600-A	83.4	15.6	0.9	ND	5.92	1.73
DP600-B	85.8	13.1	1.1	ND	5.04	1.27
DP980 [41]	30.0	70.0	ND	ND	–	–
TRIP780 [40]	72.4	3.3	10.4	13.9	4.34	1.40

ND not detected, – not measured

carbon levels [44]. Being 0.25 wt% of carbon in this TRIP steel, it can be assume that most of the austenite would have been transformed. Due to which the density of the material decreases and thus degrades the modulus of elasticity.

4 Conclusion

The paper deals with the elastic behavior of considered AHSS material. For this, specimens were loaded and unloaded in uniaxial tension in 0°, 45°, and 90° to rolling direction. The results were analyzed and compared. The

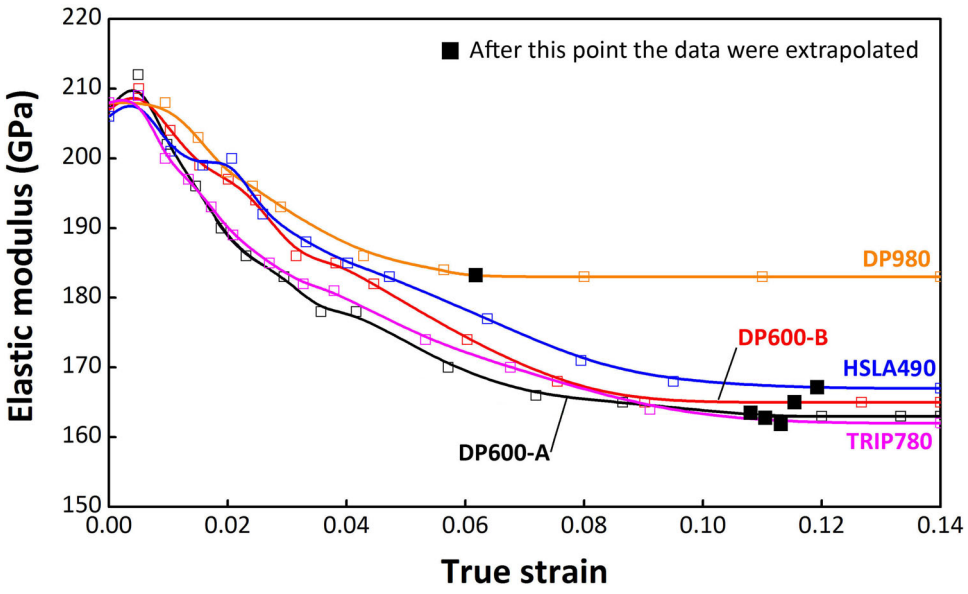

Fig. 9 Elastic modulus during unloading versus plastic strain in rolling direction

effect of plastic strain, anisotropy, and initial microstructure on reduction in elastic modulus was explained. Overall, it is concluded that:

- All presented materials show the reduction inelastic modulus during unloading and after loading. While comparing conventional steel with AHSS, the greater reduction in the elastic modulus was found for the material with higher strength. DP980 has been the exceptional material with less reduction in elastic modulus, even though it was the highest in the strength. The different behaviors of DP980 steel can be credited to the microstructure that shows the large percentage of inter-granular ferrite in martensitic matrix.
- While comparing among AHSS, it was observed that the percentage of ferrite shows a great influence on the reduction of the elastic modulus during unloading.
- The grain size between similar strength of AHSS steels influences the reduction in elastic modulus. Decrease in grain size increases the dislocation density, which further increases the micro-plastic strain and thus degrades the elastic modulus.
- Increase in martensite volume fraction in ferrite matrix increases the interface residual stress and thus decreases in elastic modulus.
- Increase in plastic strain increases the micro-cracks and thus lowers the density of the material results in decreases in elastic modulus. This is the most influential factor in TRIP steel as volume of the material increases with austenite transformation that can affect the quantitative value of elastic modulus.
- Elastic anisotropy was found in all considered material. It was found that HSLA490 saturates its anisotropy after a strain value of 0.09, but all other AHSS steels show significant anisotropy until failure. The exception is DP600-A, where the anisotropy saturates at 0.07 and continues until 0.09 and then flipped its anisotropy trend with no saturation until failure.
- The elastic recovery differences occurred between directions in all materials due to anisotropy. The maximum elastic difference occurred was with DP600-B and can also be noted from r value table. Thus, understanding of unloading and after loading elasticity is important as well as the knowledge of elastic anisotropy is also critical to model the springback.

Acknowledgements The authors thank the Usiminas and Arcelor Mittal companies for supplying the steels used in this study and CNPq Agency (Brazil) for a grant.

References

1. Nikhare C, Weiss M, Hodgson PD (2009) Crash investigation of side intrusion beam during high and low pressure tube hydroforming. In: Proceedings of international conference of tube hydroforming conference, pp 107–112
2. Bernert W et al (2008) Advanced high-strength steel product and process applications guidelines. Auto/steel partnership
3. Asgari SA et al (2008) Statistical analysis of finite element modeling in sheet metal forming and springback analysis. J Mater Proc Technol 203(1):129–136
4. Nikhare C et al (2008) Experimental and numerical evaluation of forming and fracture behaviour of high strength steel. In: Proceedings of the conference on new developments on mettalurgy and applications of high strength steels
5. Placidi F et al (2008) An efficient approach to springback compensation for ultra high strength steel structural components for the automotive field. In: International conference on new

developments on metallurgy and applications of high strength steels, Buenos Aires
6. Gan W, Wagoner RH (2004) Die design method for sheet springback. Int J Mech Sci 46(7):1097–1113
7. Tekıner Z (2004) An experimental study on the examination of springback of sheet metals with several thicknesses and properties in bending dies. J Mater Proc Technol 145(1):109–117
8. Broggiato GB et al (2012) Comparison between two experimental procedures for cyclic plastic characterization of high strength steel sheets. J Eng Mater Technol 134(4):041008-1-9
9. Viswanathan V, Kinsey B, Cao J (2003) Experimental implementation of neural network springback control for sheet metal forming. J Eng Mater Technol 125(2):141–147
10. Choi KS et al (2009) Influence of manufacturing processes and microstructures on the performance and manufacturability of advanced high strength steels. J Eng Mater Technol 131(4):041205-1-9
11. Sung JH, Kim JH, Wagoner RH (2012) The draw-bend fracture test and its application to dual-phase and transformation induced plasticity steels. J Eng Mater Technol 134(4):041015-1-15
12. Worldautosteel (2009) Advanced high strength steel (AHSS) application guidelines 4. www.worldautosteel.org
13. Andersson A (2005) Numerical and experimental evaluation of springback in a front side member. J Mater Proc Technol 169(3):352–356
14. Sever NK et al (2012) Springback prediction in bending of AHSS-DP 780. In: Proceedings of NAMRI/SME 40
15. Lems W (1963) The change of Young's modulus after deformation at low temperature and its recovery. Doctoral dissertation, TU Delft, Delft University of Technology
16. Morestin F, Boivin M (1996) On the necessity of taking into account the variation in the Young modulus with plastic strain in elastic–plastic software. N Eng Des 162(1):107–116
17. Cleveland RM, Ghosh AK (2002) Inelastic effects on springback in metals. Int J Plast 18(5):769–785
18. Luo L, Ghosh AK (2003) Elastic and inelastic recovery after plastic deformation of DQSK steel sheet. J Eng Mater Technol 125(3):237–246
19. Yang M, Akiyama Y, Sasaki T (2004) Evaluation of change in material properties due to plastic deformation. J Mater Proc Technol 151(1):232–236
20. Perez R, Benito JA, Prado JM (2005) Study of the inelastic response of TRIP steels after plastic deformation. ISIJ Int 45(12):1925–1933
21. Benito JA et al (2005) Change of Young's modulus of cold-deformed pure iron in a tensile test. Metall Mater Trans A 36(12):3317–3324
22. Kim H et al (2013) Nonlinear elastic behaviors of low and high strength steels in unloading and reloading. Mater Sci Eng A 562:161–171
23. Chongthairungruang B et al (2012) Experimental and numerical investigation of springback effect for advanced high strength dual phase steel. Mater Des 39:318–328
24. Kim H et al (2011) Effects of variable elastic modulus on springback predictions in stamping advanced high-strength steels (AHSS). In: 10th International Conference on Technology of Plasticity (ICTP) pp 628–633. ISBN: 978-3-514-00784-0
25. Toros S, Polat A, Ozturk F (2012) Formability and springback characterization of TRIP800 advanced high strength steel. Mater Des 41:298–305
26. Chongthairungruang B et al (2012) Experimental and numerical investigation of springback effect for advanced high strength dual phase steel. Mater Des 39:318–328
27. Yang X, Choi C, Sever NK, Altan T (2016) Prediction of springback in air-bending of advanced high strength steel (DP780) considering Young's modulus variation and with a piecewise hardening function. Int J Mech Sci 105:266–272
28. Ghaei A, Green DE, Aryanpour A (2015) Springback simulation of advanced high strength steels considering nonlinear elastic unloading–reloading behavior. Mater Des 88:461–470
29. Song JH, Huh H, Kim SH (2007) Stress-based springback reduction of a channel shaped auto-body part with high-strength steel using response surface methodology. J Eng Mater Technol 129(3):397–406
30. Lim H et al (2012) Time-dependent springback of advanced high strength steels. Int J Plast 29:42–59
31. Sung JH, Kim JH, Wagoner RH (2010) A plastic constitutive equation incorporating strain, strain-rate, and temperature. Int J Plast 26(12):1746–1771
32. Sun L, Wagoner RH (2011) Complex unloading behavior: nature of the deformation and its consistent constitutive representation. Int J Plast 27(7):1126–1144
33. Sun L, Kim JH, Wagoner RH (2009) Non-proportional loading of dual-phase steels and its constitutive representation, IDDRG. School Mines, Colorado
34. Gan W, Babu SS, Kapustka N, Wagoner RH (2006) Microstructural effects on the springback of advanced high-strength steel. Metall Mater Trans A 37(11):3221–3231
35. Lajarin SF, Marcondes PV (2013) Influence of computational parameters and nonlinear unloading behavior on springback simulation. J Braz Soc Mech Sci Eng 35(2):123–129
36. Cobo MR, Pla M, Hernández Rossi R, Páramo B, Antonio J (2009) Analysis of the decrease of the apparent Young's modulus of advanced high strength steels and its effect in bending simulations. In: IDDRG 2009 international conference, pp 109–117
37. NBR 6673, Flat steel products—determination of the mechanical properties of traction, ABNT, Rio de Janeiro, July 1981 (**in Portugues**)
38. Yoshida F, Uemori T (2002) A model of large-strain cyclic plasticity describing the bauschinger effect and work hardening stagnation. Int J Plast 18:661–686
39. Yoshida F, Uemori T, Fujiwara K (2002) Elastic–plastic behaviour of steel sheets underin-plane cyclic tension-compression at large strain. Int J Plast 18:633–659
40. Oliver S, Jones TB, Fourlaris G (2007) Dual phase versus TRIP strip steels: microstructural changes as a consequence of quasi-static and dynamic tensile testing. Mater Charact 58(4):390–400
41. Wang W et al (2013) Experimental study on high strain rate behavior of high strength 600–1000 MPa dual phase steels and 1200 MPa fully martensitic steels. Mater Des 47:510–521
42. Eggertsen PA, Mattiasson K (2010) On constitutive modeling for springback analysis. Int J Mech Sci 52(6):804–818
43. Chatterjee S (2006) Transformation in TRIP-assisted steels: microstructure and properties. Ph.D. thesis, Darwin College, University of Cambridge
44. www.worldautosteel.org